Supplementary Information for

Hydrogen absorption boosting in mildly annealed bulk MoS_2

Jairo Obando-Guevara,[1,2,*] Álvaro González-García,[1] Marcin Rosmus,[3] Natalia Olszowska,[3] César González,[1,4] Guillermo Morón-Navarrete,[1] Jun Fujii,[5] Antonio Tejeda,[2] Miguel Ángel González-Barrio,[1] and Arantzazu Mascaraque[1]

[1] *Dto. de Física de Materiales, Universidad Complutense de Madrid, 28040 Madrid, Spain.*

[2] *Laboratoire de Physique des Solides, CNRS, Université Paris-Saclay, 91405 Orsay, France.*

[3] *National Synchrotron Radiation Centre SOLARIS, Jagiellonian University, Czerwone Maki 98, PL-30392 Kraków, Poland.*

[4] *Instituto de Magnetismo Aplicado UCM-ADIF, E-28232 Las Rozas de Madrid, Spain*

[5] *Istituto Officina dei Materiali (IOM)-CNR, Laboratorio TASC. I-34149 Trieste, Italy.*

(Dated: July 4, 2024)

Keywords: hydrogen adsorption, defects engineering, two-dimensional material, angle-resolved photoemission spectroscopy, DFT.

* jairoban@ucm.es

I. Comparison of the valence band of an undoped and a Nb-doped MoS_2 sample

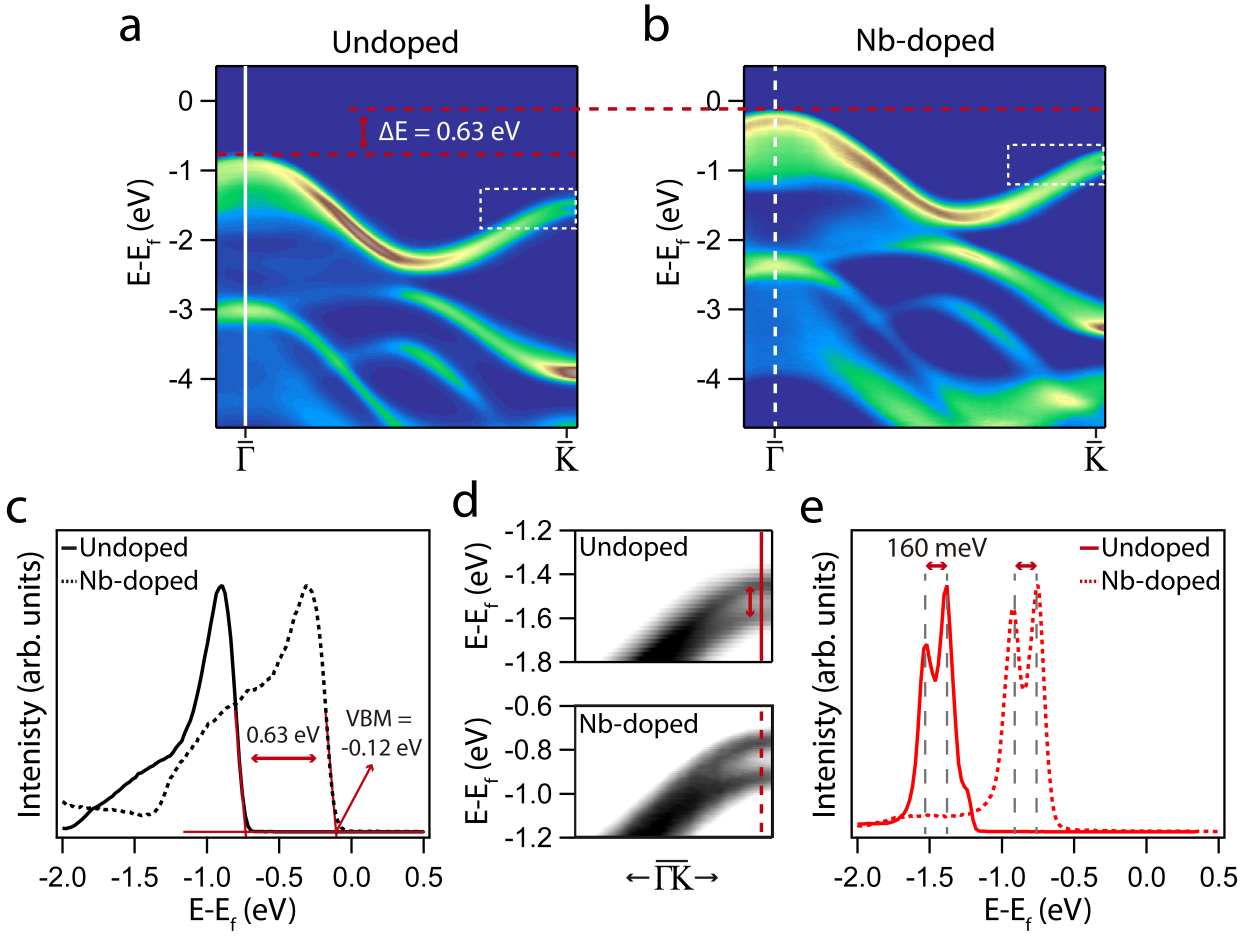

FIG. S1. (a-b) ARPES intensity showing the dispersion along the $\overline{\Gamma K}$ direction for the undoped and Nb-doped samples, respectively. The aceptor dopant density is $N_a \sim 2 \cdot 10^{17}$ cm^{-3}. (c) Energy dispersion curves (EDCs) at the $\overline{\Gamma}$ point marked in (a-b) showing the VBM determination of the undoped (white continuous line) and Nb-doped (white dashed line) samples. A rigid band shift of 0.63 eV towards the Fermi level is obtained. The EDCs integrate a $\Delta k_{||} = 0.1$ Å^{-1} region centered at $\overline{\Gamma}$. (d) Detail of the ARPES intensity around the $\overline{\text{K}}$ point of the undoped (top) and Nb-doped (bottom) samples highlighting the splitting at this point. The displayed region corresponds to the white dashed boxes in panels (a-b). (e) EDCs at the $\overline{\text{K}}$ point marked in (d) showing a spin-orbit splitting of 160 meV in the undoped (red continuous line) and Nb-doped (red dashed line) samples. The EDCs integrate a $\Delta k_{||} = 0.06$ Å^{-1} region centered at $\overline{\text{K}}$.

II. Comparison of the core-levels of an undoped and Nb-doped MoS_2 sample

In Fig. S2a-b we depict the X-ray photoemission spectroscopy (XPS) of the Mo $3d$ and S $2p$ series of core-levels (CL) for both the undoped and Nb-doped samples. Three peaks are identified after fitting the spectrum of Fig. S2a. In the undoped (Nb-doped) sample, the S $2s$ peak is observed at 226.41 eV (225.93 eV), the Mo $3d_{5/2}$ peak at 229.21 eV (228.73 eV), corresponding to Mo^{+4} oxidation state in MoS_2, and a minor peak, the Mo $3d_{3/5}$ at 232.35 eV (231.83 eV), due to Mo^{+6} oxidation state in MoO_3. The presence of MoO_3 can be attributed to the use of MoO_3 as a precursor agent during the chemical vapour transport (CVT) growth. Fig. S2b presents the S $2p$ peak and its corresponding fitting. In the undoped (Nb-doped) sample, the S $2p_{3/2}$ component is at 162.05 eV (161.54 eV).

A summary of the peak shifts is presented in Fig. S2c, for the main MoS_2 CL peaks: 0.48 eV for Mo $3d_{3/5}$ and 0.51 eV for S $2p$. It is important to note that no Nb $3d$ signal was detected in any of the doped sample batches employed in this work (see Fig. S2d). As said before, the Nb doping concentration is $\sim$0.001 at.% (i.e., $\sim 2 \cdot 10^{17}$ cm^{-3}), so it is notably lower in comparison to concentrations used in other works[1,2]. In these studies, for a doping concentration of 0.5 at.% and higher, well-resolved Nb $3d$ CL is detected.

Therefore, we do not observe changes in the VB or the core-levels due to Nb doping. Both undoped and Nb-doped samples exhibit similar characteristics.

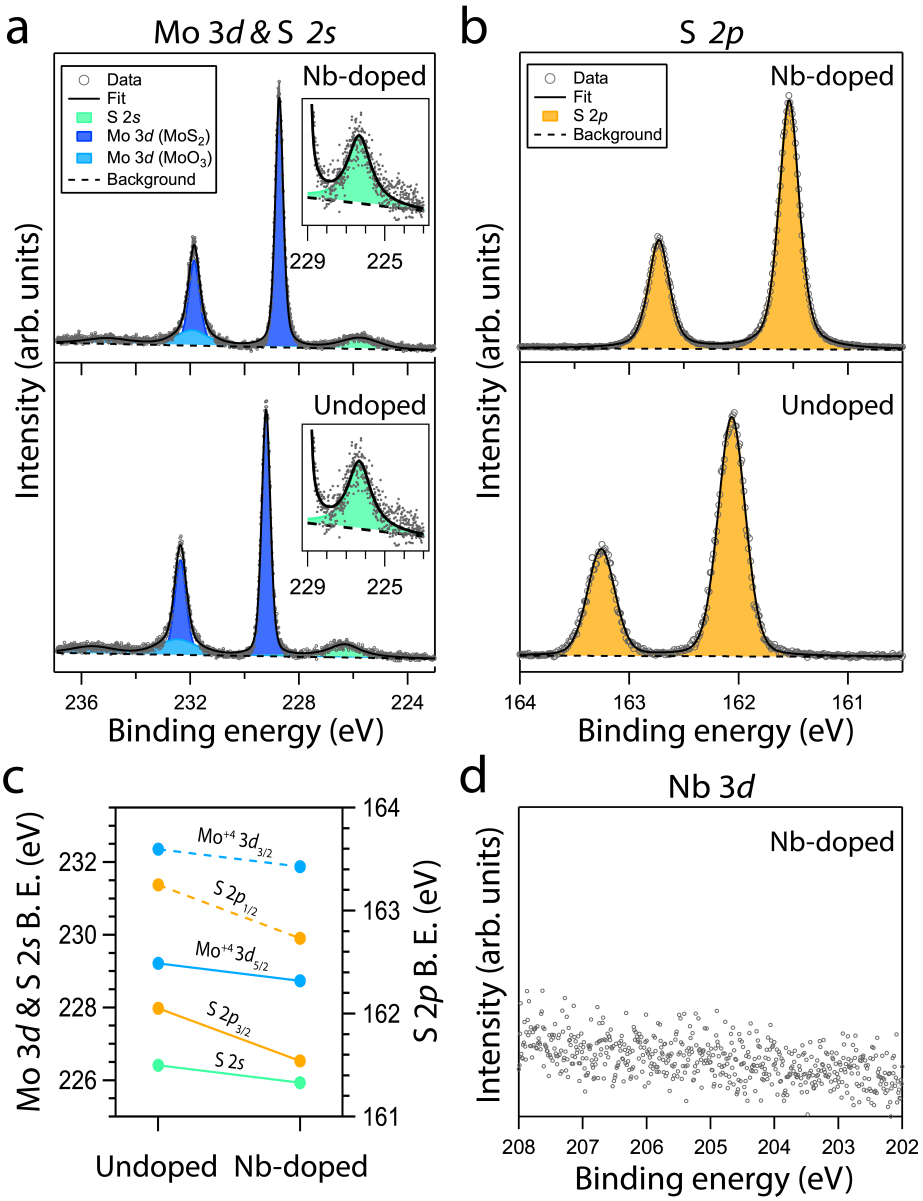

FIG. S2. XPS CLs of the undoped and undoped MoS_2 samples. (a) Mo 3*d* & S 2*s*. Inset: S 2*s* ($h\nu = 400$ eV). (b) S 2*p* ($h\nu = 200$ eV). (c) Summary of the peak shifts of the fitted components in (a-b). (d) Nb 3*d* ($h\nu = 400$ eV).

III. DFT band structure of a pristine single-layer of MoS_2 and a single-layer with H atoms adsorbed in the V_S

In Fig. S3a-b we present the calculated band structure of the pristine MoS_2 structure and the structure with two H atoms adsorbed onto the V_S (4 % of V_S), respectively. The calculation of panel b was performed using the unfolding package adapted to Quantum Espresso.

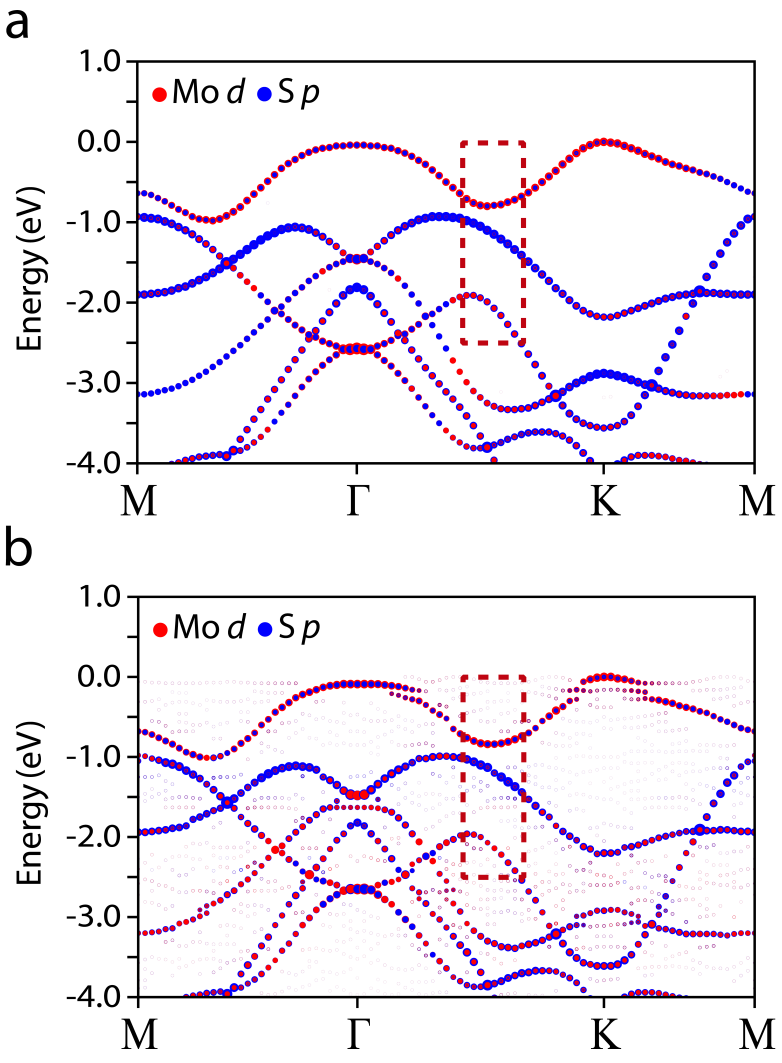

FIG. S3. (a) DFT orbital-projected electronic band structure calculated for a pristine single-layer of MoS_2. (b) DFT orbital-projected electronic band structure calculated for a single-layer of MoS_2 with H atoms adsorbed and with 4 % of V_S. The red dashed rectangles marks the region from which the set of EDCs of Fig. 3d and Fig. 4d are taken.

To simulate the impact of the exposure to H_2 of a surface with sulfur vacancies, various adsorption configurations were examined. Since the evolution of the band structure after annealing indicates that the created sulfur defect density is not very high, a 4% of V_S was introduced accordingly. First, we observed that in the pristine scenario (no V_S) the H_2 molecule prefers to physisorb on top sites of the Mo atoms (T_{MO}) with a vertical orientation. When V_S defects are introduced, the H_2 molecule tends to occupy the V_S position. However, the outcome depends on the molecule orientation. Vertically oriented H_2 favours physisorption, adopting an equilibrium position ~ 1.8 Å above the top S layer. Conversely, when the molecule is forced to lie horizontally close to a V_S, it also dissociates. The resulting H atoms bond to the uncoordinated Mo atoms. The dissociation scenario is 0.17 eV more favourable than physisorption. Additional configurations were tested by placing one and three hydrogen atoms in the V_S (not shown). These configurations are less energetically favourable[3].

IV. Detail of the formation of a Fermi step after hydrogenation

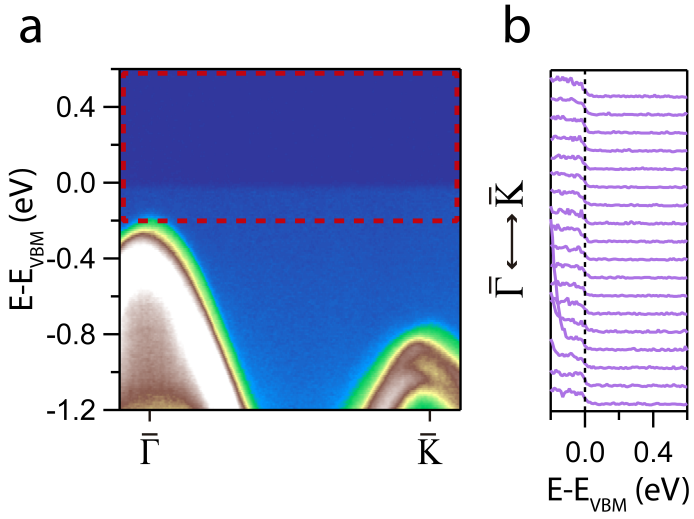

FIG. S4. (a) Enlarged region of Fig. 4a, showing details of the ARPES intensity along the $\overline{\Gamma K}$ direction for the annealed sample at 700 °C after exposure to 1000 L of H_2 at a pressure of $1 \cdot 10^{-4}$ mbar ("high pressure"). (b) Set of EDCs taken in the red rectangle region marked in (a). The EDCs show the formation of a Fermi step after hydrogenation through the entire reciprocal space.

V. Comparison between the hydrogenation at relative high and low pressures

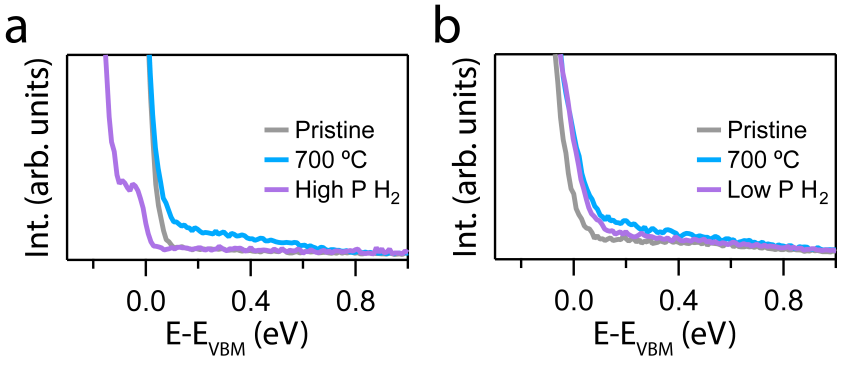

FIG. S5. Enlarged region of the EDC at $\overline{\Gamma}$ of the sample hydrogenated after annealing at 700 °C. (a) Hydrogenation at $1 \cdot 10^{-4}$ mbar ("high pressure" up to 1000 L and RT. (b) Hydrogenation at $1 \cdot 10^{-6}$ mbar ("low pressure") up to 1000 L. The pristine and 700 °C annealing EDCs are included for comparison.

[1] J. Suh, T.-E. Park, D.-Y. Lin, D. Fu, J. Park, H. J. Jung, Y. Chen, C. Ko, C. Jang, Y. Sun, R. Sinclair, J. Chang, S. Tongay, and J. Wu, Nano Letters **14**, 6976 (2014).

[2] M. R. Laskar, D. N. Nath, L. Ma, E. W. Lee, C. H. Lee, T. Kent, Z. Yang, R. Mishra, M. A. Roldan, J.-C. Idrobo, S. T. Pantelides, S. J. Pennycook, R. C. Myers, Y. Wu, and S. Rajan, Applied Physics Letters **104**, 092104 (2014).

[3] Y. Irusta, G. Morón-Navarrete, and C. Gonzalez, Nanotechnology (2024).